POLITECNICO DI TORINO
Repository ISTITUZIONALE

Human-impacted waters: New perspectives from global high-resolution monitoring

Original
Human-impacted waters: New perspectives from global high-resolution monitoring / Ceola, S., Laio, F., Montanari, A.. - In: WATER RESOURCES RESEARCH. - ISSN 0043-1397. - STAMPA. - 51:9(2015), pp. 7064-7079. [10.1002/2015WR017482]

Availability:
This version is available at: 11583/2626764 since: 2015-12-22T15:01:02Z

Publisher:
American Geophysical Union:2000 Florida Avenue Northwest:Washington, DC 20009:(800)966-2481,

Published
DOI:10.1002/2015WR017482

Terms of use:

This article is made available under terms and conditions as specified in the corresponding bibliographic description in the repository

Publisher copyright

(Article begins on next page)

07 October 2026

AGU PUBLICATIONS

Water Resources Research

RESEARCH ARTICLE
10.1002/2015WR017482

Special Section:
The 50th Anniversary of Water Resources Research

Human-impacted waters: New perspectives from global high-resolution monitoring

Serena Ceola[1], Francesco Laio[2], and Alberto Montanari[1]

[1]Department of Civil, Chemical, Environmental and Materials Engineering, University of Bologna, Bologna, Italy, [2]Dipartimento di Ingegneria dell'Ambiente, del Territorio e delle Infrastrutture, Politecnico di Torino, Turin, Italy

Key Points:
- Fine-scale remotely sensed nightlights provide new perspectives in water science
- Spatiotemporal trends of human proximity to rivers from 1992 to 2013 are analyzed from nightlights
- The human presence close to rivers, derived from nightlights, increased from 1992 to 2013

Supporting Information:
- Supporting Information S1
- Table S1

Correspondence to:
S. Ceola,
serena.ceola@unibo.it

Citation:
Ceola, S., F. Laio, and A. Montanari (2015), Human-impacted waters: New perspectives from global high-resolution monitoring, *Water Resour. Res.*, *51*, 7064–7079, doi:10.1002/2015WR017482.

Received 30 APR 2015
Accepted 25 JUL 2015
Accepted article online 31 JUL 2015
Published online 2 SEP 2015

This article was corrected on 18 Jan 2016. See the end of the full text for details.

Abstract The human presence close to streams and rivers is known to have consistently increased worldwide, therefore introducing dramatic anthropogenic and environmental changes. However, a spatio-temporal detailed analysis is missing to date. In this paper, we propose a novel method to quantify the temporal evolution and the spatial distribution of the anthropogenic presence along streams and rivers and in their immediate proximity at the global scale and at a high-spatial resolution (i.e., nearly 1 km at the equator). We use satellite images of nocturnal lights, available as yearly snapshots from 1992 to 2013, and identify five distinct distance classes from the river network position. Our results show a temporal enhancement of human presence across the considered distance classes. In particular, we observed a higher human concentration in the vicinity of the river network, even though the frequency distribution of human beings in space has not significantly changed in the last two decades. Our results prove that fine-scale remotely sensed data, as nightlights, may provide new perspectives in water science, improving our understanding of the human impact on water resources and water-related environments.

1. Introduction

The ongoing human impact enhancement on the environment and particularly on water resources is posing challenging questions and opportunities in the context of environmental planning and management. The main reasons of concern are related to the overexploitation of water resources and the increase of water-related hazards, which are strictly linked to the increase in population density close to water bodies [*Vorosmarty et al*., 2010]. The systematic anthropogenic presence close to perifluvial areas dates back to 4000 B.C., when ancient populations settled close to major rivers, like the Nile, the Tigris, and the Euphrates [*Rogers*, 2007]. As humans needed to benefit from water, they began to control and manage fluvial water resources for civil use and irrigation purposes, albeit river intakes generally lead to a modification of the natural river flow regime in terms of quantitative and qualitative alterations of river discharge, with cascade effects on the fluvial ecosystem [*Poff et al*., 1997; *Vorosmarty et al*., 2010; *Ceola et al*., 2013]. Human exploitation of water resources has steadily increased in time, to the point that the actual geological era has been defined the Anthropocene [*Crutzen*, 2002], with humans exerting a crucial control, significantly greater than in the past, on nature and hydrology in particular. Indeed, humans play a key role as an integral component in the Earth system, and they cannot longer be considered a mere external factor [*Vorosmarty et al*., 2010; *Rockstrom et al*., 2014]. In particular, an increasing need to better understand the dynamics of coupled human-water systems, and consequently provide quantitative indicators to estimate the human influence, has been recently clearly recognized by the scientific community [*Sivapalan et al*., 2012; *Montanari et al*., 2013; *Di Baldassarre et al*., 2013, 2015; *Erisman et al*., 2015].

The proximity of populations to streams and rivers is a source of major concern in the context of flood risk, water pollution, anthropogenic use of natural water resources, as well as for measuring the possible increase of human pressure on river ecosystems. Anthropogenic, climate, and geomorphic changes are widely recognized to influence and control the global water change [*IPCC*, 2013; *UNISDR*, 2013; *Jaramillo and Destouni*, 2014; *Slater et al*., 2015]. More specifically, climate change, as epitomized by several scientific studies, may cause river flow alterations [*Vorosmarty et al*., 2000; *Barnett et al*., 2008; *Hirabayashi et al*., 2013; *Kundzewicz et al*., 2014; *Berghuijs et al*., 2014]. *Barnett et al*. [2008], for instance, observed a significant change in the hydrological cycle of western United States between 1950 and 1999, characterized by a modification in the mountain precipitation features with consequent changes in river discharge. Water changes are also

© 2015. American Geophysical Union. All Rights Reserved.

associated with a variability in landscape conditions and land use [*Slater et al*., 2015]. To corroborate this point, *Jaramillo and Destouni* [2014] recognized that river flow modifications rely both on landscape and climate drivers, where, interestingly, the effects of landscape drivers often overcome the climate ones. Moreover, anthropogenic changes, resulting from population dynamics, urbanization processes, socioeconomic, and cultural developments, may drive as well significant modifications of water cycle dynamics [*Vorosmarty et al*., 2000; *Haddeland et al*., 2014]. In particular, the anthropogenic presence close to rivers has experienced an evolution in time characterized by an enhancement of the human pressure and proximity to streams and rivers over the past decades [*Becker and Grunewald*, 2003; *Jongman et al*., 2012; *Ceola et al*., 2014].

Although the human pressure on water resources is exerted at the local level, the aggregation of anthropogenic impacts at large scale is inducing a worldwide water emergency that should be addressed and studied at the global level. We argue in this paper that the new generation of fine-scale remotely sensed data, such as, for instance, those provided by the Gravity Recovery and Climate Experiment (GRACE) and Landsat, is paving the way for developing innovative environmental and water resources monitoring opportunities, which move beyond the traditional use of hydrological variables [see *Voss et al*., 2013; *Richey et al*., 2015]. However, a technically useful assessment of the status of water resources needs to be based on fine-scale multifaceted information, by making a comprehensive use of several alternative sources of new data.

In this context, recent efforts toward a worldwide analysis on how people live close to fluvial waterbodies and how this process changed in time have been pursued. We may recall, for instance, the contribution by *Small* [2004], who analyzed how the global population is spatially distributed by considering both 1990 census information and 2004–2005 nighttime lights, but also the one by *Kummu et al*. [2011], who proposed a global analysis of population distance to freshwater bodies by using the Landscan 2007 population density data set aggregated at a 5 km resolution. Even though they thoroughly studied how population distance relates to climatic zones and administrative boundaries, their database did not allow for the investigation of the progress in time of human pressure on rivers. Here we present a novel approach for (i) evaluating the spatial distribution of human settlements and economic activity close to fluvial waterbodies, (ii) quantifying the average human proximity to rivers, and (iii) identifying their temporal evolution by using nighttime lights.

The paper is organized as follows: section 2 outlines the underlying motivations of the present study, while section 3 presents the nightlight and river network data sets employed for the analysis, as well as the methodology proposed for the identification of distance-from-river classes and the analysis of geographical and human spatial distribution and proximity to rivers. The main outcomes of the analysis, focused at increasingly finer spatial scales, are presented and discussed in section 4, while a discussion and some final remarks are reported in section 5.

2. Motivation of the Study

We aim to support the development of an innovative vision for assessing the status of water resources and water-related risk, by promoting the global analysis of local scale problems, therefore bridging the scale gap between the point occurrence of single environmental emergencies and the large spatial scale (up to the global one) typically characterizing environmental assessment and planning. Approaching the problem at a large scale is necessary in view of the need to make a comprehensive assessment of existing risks and develop an efficient planning of interventions. On the other hand, to devise technically useful solutions one needs to refer to the point scale. One of the keys to bridge this scale gap is provided by global, fine-scale environmental data sets, which offer exciting perspectives that are not yet fully exploited in the context of water resources and water-related risks. In particular, hydrologists should consider the opportunities given by innovative information that goes beyond the variables that are traditionally used in hydrology. An effort should be made to exploit the opportunities given by the multitude of fine-scale environmental information that is nowadays available at the global level.

In this paper, we provide a first example that shows the opportunities provided by nightlight data to better decipher the interaction between human and water systems. Following a traditional approach, nightlight would not be deemed to provide any hydrologic information. Conversely, we herein show that they can indeed be very useful, provided that one embraces a new vision where the hydrologic system, and the related control volume, is extended to include other closely connected dynamical systems.

Table 1. Nighttime Lights Data Set, Satellite Number, and Observation Year[a]

	F10	F12	F14	F15	F16	F18
1992	F101992					
1993	F101993					
1994	F101994	F121994				
1995		F121995				
1996		F121996				
1997		F121997	F141997			
1998		F121998	F141998			
1999		F121999	F141999			
2000			F142000	F152000		
2001			F142001	F152001		
2002			F142002	F152002		
2003			F142003	F152003		
2004				F152004	F162004	
2005				F152005	F162005	
2006				F152006	F162006	
2007				F152007	F162007	
2008					F162008	
2009					F162009	
2010						F182010
2011						F182011
2012						F182012
2013						F182013

[a]In case of satellites operating simultaneously, a new nightlight product is evaluated as the average of overlapped satellites (i.e., for years 1994, 1997, 1998, 1999, 2000, 2001, 2002, 2003, 2004, 2005, 2006, 2007).

3. Materials and Methods

3.1. Nighttime Light Data Set

Nighttime light time series, collected by the US Air Force Weather Agency under the Defense Meteorological Satellite Program (DMSP)—Operational Linescan System (OLS), are provided as freely available digital products by the National Geophysical Data Center from the National Oceanic and Atmospheric Administration (NOAA). Nightlight data, produced on a yearly basis from 1992 to 2013, represent cloud-free nocturnal luminosity from sites with protracted lighting (i.e., cities, towns, gas flares). Sunlit and moonlit data and observations from ephemeral phenomena like fires are excluded from the data set. Nightlight values, expressed as a digital number *DN*, range from 0 to 63, corresponding to conditions characterized by absence of lights and pronounced luminosity, respectively. Nightlights thus represent a valuable proxy for the presence of human settlements and economic activity and they have been widely employed for demographic, economic, and environmental purposes [*Elvidge et al*., 1997, 2009; *Small*, 2004; *Chand et al*., 2009; *Chen and Nordhaus*, 2011; *Bennie et al*., 2014]. Recently, *Ceola et al*. [2014] used nightlights data to show that nocturnal lights close to streams and rivers are significantly related to economic losses due to flood events. In particular, they found that more significant flood damages took place across the more illuminated areas.

Nightlights cover almost the entire world (180°W–180°E longitude, 75°N–65°S latitude) and they are available as raster products at a very detailed spatial resolution, i.e., 30 arc sec, corresponding to nearly 1 km at the equator. Six different satellites collected the nighttime light data set (Table 1). For some years, two different satellites were operating simultaneously and produced two distinct nightlight products. In order to get a unique and representative nightlight value for each pixel and for each year, we evaluated the average nocturnal luminosity from the two overlapped data sets. Because raw nightlight data are not on-board calibrated and cannot be compared among the 22 year period, a preliminary intercalibration procedure is required. Therefore, we empirically intercalibrated yearly averaged nightlights, following a procedure widely applied in the scientific literature [*Elvidge et al*., 2009; *Chen and Nordhaus*, 2011]. In addition, we excluded all data associated to gas flares, deemed to be irrelevant for the analysis of human proximity to streams and rivers.

3.2. River Network Data Set

We employed the HydroSHEDS data set to geographically locate the river network at the global scale [*Lehner et al*., 2008, http://www.worldwildlife.org/hydrosheds, http://hydrosheds.cr.usgs.gov]. The HydroSHEDS

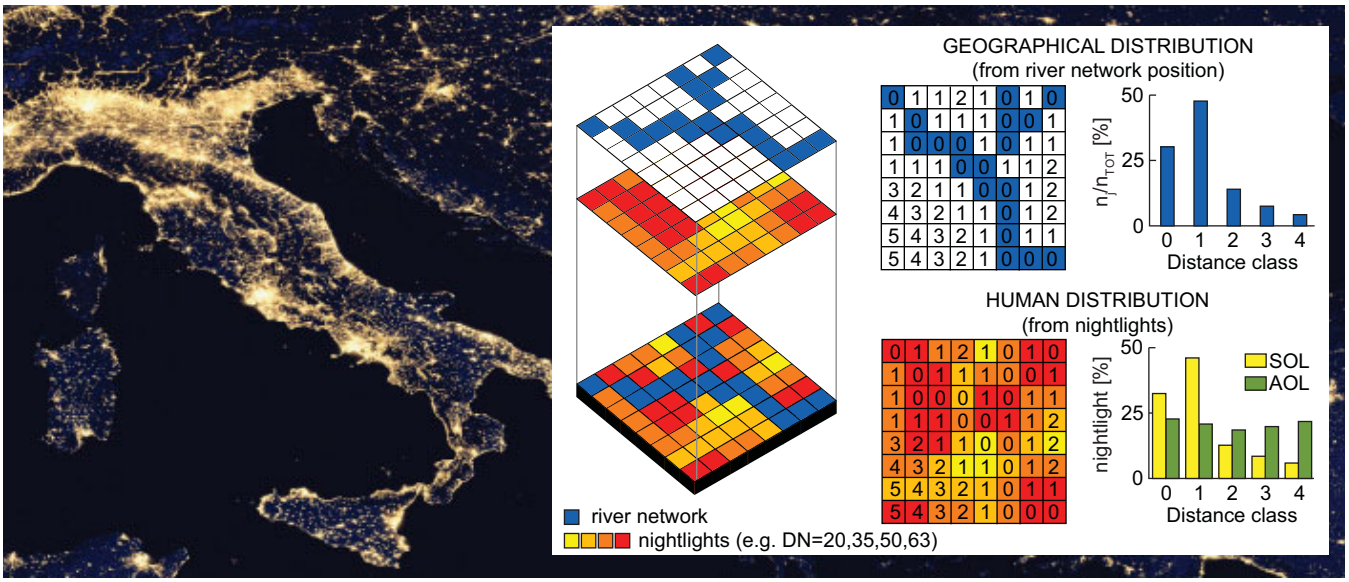

Figure 1. Nightlight identification method for the considered distance-from-river classes: 2012 nightlight satellite image for the Italian region (from https://earthdata.nasa.gov/labs/overview), and (inset) an example showing (i) distance class delineation from the river network position, with associated distribution of pixel class abundance, and (ii) nightlight analysis in terms of total (SOL) and average (AOL) nocturnal luminosity values.

river network is derived from the SRTM digital elevation model properly reconditioned in specific cases (i.e., void-filled and hydrologically conditioned). The data set, available as a vector file, presents the same spatial resolution as nightlight images (i.e., 30 arc sec), though it has a smaller extension (138°W–180°E longitude, 62°N–55°S latitude). In particular, Canada, Russia, Norway, Sweden, Island, and Finland are not included in the data set extent. Even though alternative and more extended river network data sets could have been used, we opted for HydroSHEDS because it refers to a superior digital elevation model that provides more accurate products. Indeed, the selected data set is widely considered a benchmark as reflected by its application including global river routing and floodplain inundations [*Gong et al*., 2011; *Yamazaki et al*., 2011; *Alfieri et al*., 2013].

3.3. Identification of Distance Classes

To identify the geographical and human distribution across streams and rivers, we defined five distinct distance-from-rivers classes. We first converted the original vectorial HydroSHEDS river network to a raster file and then outlined the following classification. River network pixels are classified as distance-0 pixels. All pixels adjacent to streams are ranked as distance-1 pixels, whereas distance-2, distance-3, and distance-4 pixels are defined from concentric zones, as outlined in Figure 1. Pixels with a distance from the HydroSHEDS river network greater than the distance-4 class are excluded from the analysis, since they represent less than 5% of the study area. The proposed approach was applied to the entire HydroSHEDS data set extent. In particular, we considered the following 175 study regions, progressively focusing on smaller scales: world (where Canada, Russia, and Northern Europe are excluded), six continents (i.e., North America, South America, Europe, Asia, Africa, and Oceania), and 168 countries having a population greater than 300,000 inhabitants (supporting information Table S1).

3.4. Spatial Distribution Analysis: Geographical Versus Human Perspective

For each of the 175 study regions, we examined how single pixels and the associated nightlight values are distributed across the considered distance classes, thus following a geographical and a human perspective, respectively. All variables defined in what follows are summarized in Table 2.

From the geographical perspective, for each study region x we computed the number of pixels $n_j(x)$ belonging to each distance class j, where j varies from 0 to 4, as well as the total number of pixels $n_{TOT}(x)$ by considering all distance classes defined as

Table 2. Summary of the Study Variables Defined for the Geographical and Human Spatial Distribution and Proximity Analyses

Analysis	Perspective	Variable	Description
Spatial distribution analysis	Geographical variables	x	Study region
		j	Distance class (j = 0,1,2,3,4)
		$n_j(x)$	Absolute pixel abundance (number of pixels) for distance class j and study region x
		$n_{TOT}(x)$	Total number of pixels within the study region x (i.e., all distance classes are considered)
		$\frac{n_j(x)}{n_{TOT}(x)}$	Relative pixel abundance (%) for distance class j and study region x
	Human variables (from nightlights)	$DN_i(x,t)$	Nightlight value for pixel i, study region x and year t
		$SOL_j(x,t)$	Absolute sum of nightlights for distance class j, study region x and year t
		$SOL_{TOT}(x,t)$	Total sum of nightlights within the study region x (i.e., all distance classes are considered) for year t
		$\frac{SOL_j(x,t)}{SOL_{TOT}(x,t)}$	Relative sum of nightlights (%) for distance class j, study region x and year t
		$AOL_j(x,t)$	Absolute average nightlight value for distance class j, study region x and year t
		$AOL_{TOT}(x,t)$	Absolute average nightlight value within the study region x (i.e., all distance classes are considered) for year t
		$\frac{AOL_j(x,t)}{AOL_{TOT}(x,t)}$	Relative average nightlight value for distance class j, study region x and year t, labeled in what follows as the *human-geographical ratio*
Proximity analysis	Geographical variables	$d_{GEO}(x)$	Average geographical proximity of randomly selected locations to the river network
	Human variables (from nightlights)	$d_{SOL}(x,t)$	Average human proximity of randomly selected human beings to the river network
		$D_{SOL^*}(x,t)$	Human distance-from-river range

$$n_{TOT}(x)=\sum_{j=0}^{4} n_j(x). \tag{1}$$

We also computed the relative pixel abundance $n_j(x)/n_{TOT}(x)$, expressed as the ratio between the absolute class abundance and the total abundance (Figure 1 and Table 2).

To account for the human distribution across distance classes, we employed the aforementioned nightlights time series, available on a yearly basis from 1992 to 2013. Similarly to the geographical distribution analysis, for each study region x and for each year t we analyzed the human distribution by first considering the absolute sum of nightlights $SOL_j(x,t)$ belonging to each distance class j, expressed as

$$SOL_j(x,t)=\sum_{i=1}^{n_j(x)} DN_i(x,t), \tag{2}$$

where $DN_i(x,t)$ identifies the nightlight value associated to the pixel i, and $n_j(x)$ represents the pixel abundance for distance class j (Figure 1 and Table 2). We also computed the total sum of nightlights within the study region by using

$$SOL_{TOT}(x,t)=\sum_{j=0}^{4} SOL_j(x,t), \tag{3}$$

and we determined the relative sum of nightlights $SOL_j(x,t)/SOL_{TOT}(x,t)$, defined as the ratio between the absolute nightlight sum $SOL_j(x,t)$ and the overall sum evaluated from the total number of considered pixels $SOL_{TOT}(x,t)$. In order to exclude the effect of pixel class abundance and thus focus only on human distribution, we normalized the sum of nightlights $SOL_j(x,t)$ by the number of pixels belonging to each distance class $n_j(x)$ and obtained an average nightlight value $AOL_j(x,t)$ (Figure 1 and Table 2). Therefore, we

considered absolute and relative average values of nightlights $AOL_j(x,t)$ and $AOL_j(x,t)/AOL_{TOT}(x,t)$, respectively, where

$$AOL_j(x,t) = \frac{SOL_j(x,t)}{n_j(x)} \tag{4}$$

and

$$AOL_{TOT}(x,t) = \frac{SOL_{TOT}(x,t)}{n_{TOT}(x)}. \tag{5}$$

In particular, we examined the spatiotemporal trend of relative average nightlight values $AOL_j(x,t)/AOL_{TOT}(x,t)$, labeled in what follows as the human-geographical ratio. When the human-geographical ratio is greater than 1, the within-class average luminosity is higher than the average across the entire study region, and the anthropogenic presence is larger than expected with the uniform density distribution. This uniform density distribution is derived from the geographical distribution $n_j(x)/n_{TOT}(x)$, where the relative human density within each distance class is equal to the relative pixel abundance. Conversely, when the human-geographical ratio is smaller than 1, the considered distance class presents an average nightlight luminosity smaller than the average across the study region, and the actual human presence is smaller compared to the uniformly distributed human density.

3.5. Proximity to Rivers: Geographical Versus Human Perspective

Moving from the spatial distribution analysis presented in the previous paragraph, for all the considered 175 study regions we defined the average proximity to rivers, both from a geographical and a human perspective. In particular, from the geographical frequency distribution analysis, we defined the average geographical proximity to the river network of randomly selected pixels, $d_{GEO}(x)$, as

$$d_{GEO}(x) = \sum_{j=0}^{4} \frac{j \cdot n_j(x)}{n_{TOT}(x)}, \tag{6}$$

where x identifies the considered study region. This proximity, measured in pixels, results from a weighed average of class abundance, with a weight equal to the relative class abundance $n_j(x)/n_{TOT}(x)$.

In a similar fashion, we also evaluated the average human proximity to the river network of randomly selected human beings, $d_{SOL}(x,t)$, derived from nightlight statistics as follows:

$$d_{SOL}(x,t) = \sum_{j=0}^{4} \frac{j \cdot SOL_j(x,t)}{SOL_{TOT}(x,t)}, \tag{7}$$

where t represents a generic year from 1992 to 2013. In this case the human proximity to rivers, measured in pixels, is a weighted average of the distance class total luminosity, where the relative sum of nightlights, $SOL_j(x,t)/SOL_{TOT}(x,t)$, represents the weight. Given that we estimated the average human proximity to the river network for each study region on a yearly basis within the study period, we applied a linear regression model to identify a possible temporal trend of $d_{SOL}(x,t)$. Therefore, we fitted $d_{SOL}(x,t)$ values versus time by using

$$d_{SOL}(x,t) = s_{d_{SOL}}(x) \cdot t + i_{d_{SOL}}(x), \tag{8}$$

where $s_{d_{SOL}}(x)$ is the slope of the regression line, representing the yearly variation of the average human proximity to the river network for each study region x, t is time, and $i_{d_{SOL}}(x)$ is the intercept. In order to test the significance of the dependence between $d_{SOL}(x,t)$ and time, we then applied the Student's t test and evaluated the correlation coefficients R and p values (see supporting information Table S1).

Furthermore, in order to check and account for temporal changes in human presence close to river bodies within the 22 year study period, we analyzed how the total sum of nightlights observed at the beginning of the study period within each study region, $SOL_{TOT}(x,1992)$, modified its spatial distribution across years from 1992 to 2013. More specifically, we first considered $SOL_{TOT}(x,1992)$, labeled in what follows $SOL^*(x)$, as our reference nightlight value, whose associated population is located by definition within all distance classes from 0 to 4. Then, for each study region and for each year we computed a new distance value, which

we called human distance-from-river range, $D_{SOL^*}(x,t)$, defined as the distance range within which the sum of nightlights equal to $SOL^*(x)$ is settled. To better clarify this concept, we provide the following example. In 1992, $SOL_{TOT}(x,1992)$, equal to the reference value $SOL^*(x)$, refers to all distance classes and thus to $D_{SOL^*}(x,1992)$ equal to 4 pixels. If $SOL_{TOT}(x,2013) > SOL^*(x)$, we can state that there has been a human presence enhancement in the study region x from 1992 to 2013, meaning that $SOL^*(x)$ in 2013 is located within a smaller distance from river, e.g., $D_{SOL^*}(x,2013)=3.15$ pixels. Note that we opted to use lower and upper capital case letters to differentiate between the average proximity of randomly selected locations or individuals and the human distance-from-river range. From an analytical view point, $D_{SOL^*}(x,t)$ can be derived from

$$\sum_{j=0}^{D_{SOL^*}(x,t)} SOL_j(x,t) = SOL^*(x). \tag{9}$$

Thus, the human distance-from-river range $D_{SOL^*}(x,t)$ is defined as follows:

$$D_{SOL^*}(x,t)=\begin{cases} k + \dfrac{SOL_k(x,t) - \left(\sum_{j=0}^{k} SOL_j(x,t) - SOL^*(x)\right)}{SOL_k(x,t)} & \text{if } SOL_{TOT}(x,t) \geq SOL^*(x), \\ 4 & \text{if } SOL_{TOT}(x,t) < SOL^*(x) \end{cases} \tag{10}$$

where k represents one of the considered distance classes for which $\sum_{j=0}^{k} SOL_j(x,t) \geq SOL^*(x)$. According to equation (10), $D_{SOL^*}(x,t)$ can assume either integer or real values, depending on the percentage of nightlights and pixels located in the k-distance class which effectively contribute to reaching a sum of nightlights equal to $SOL^*(x)$. Finally, we determined the temporal evolution of $D_{SOL^*}(x,t)$ through a linear regression model, by employing the ordinary least squares error method to estimate the regression coefficients. The regression model reads

$$D_{SOL^*}(x,t) = s_{D_{SOL^*}}(x) \cdot t + i_{D_{SOL^*}}(x), \tag{11}$$

where $s_{D_{SOL^*}}(x)$ represents the slope of the regression line (i.e., yearly variation of human distance-from-river range) and $i_{D_{SOL^*}}$ is the intercept. We also verified that the linear regression model significantly reproduced $D_{SOL^*}(x,t)$ data by computing the correlation coefficients R and p values for the Student's t test (see supporting information Table S1).

Note that, from the geographical perspective, the spatial distribution and average proximity to rivers are strictly related to the position of single pixels with respect to the river network location within the considered study regions. No insights about human presence or details on a temporal evolution are provided, since this information is geographically based and time-invariant. Conversely, the spatial distribution, the average proximity to rivers and the human distance-from-river range derived from nightlight data offer interesting hints supporting the analysis of anthropogenic presence close to streams and rivers, thus allowing the study of its temporal evolution in the period from 1992 to 2013.

4. Results

4.1. Geographical and Human Spatial Distributions Across Distance Classes

To study how the geographical distribution varies among the considered regions, we analyzed the $n_j(x)/n_{TOT}(x)$ histograms. Our results revealed that almost all study regions (i.e., world, continents, and the majority of countries) present a hump-shaped trend in terms of relative pixel frequency for each distance class, with a mode for distance-1 class (see inset histograms in Figure 2, showing global and continental geographical frequency distributions). Nevertheless, a few exceptions occurred: an increasing trend, with the majority of pixels in distance-4 class, characterized small-extension countries such as Bahrain, Comoros, Hong Kong, Malta, and Singapore. These outcomes clearly depend on the geomorphological features and the spatial resolution from which the selected river network (i.e., HydroSHEDS) has been delineated. Originally, the HydroSHEDS river network was derived at a 3 arc sec resolution, but coarser resolutions were provided through an upscaling procedure to be easily employed at the global scale. The upscaled river network at 30 arc sec resolution used for the present analysis is significantly well aligned with the original

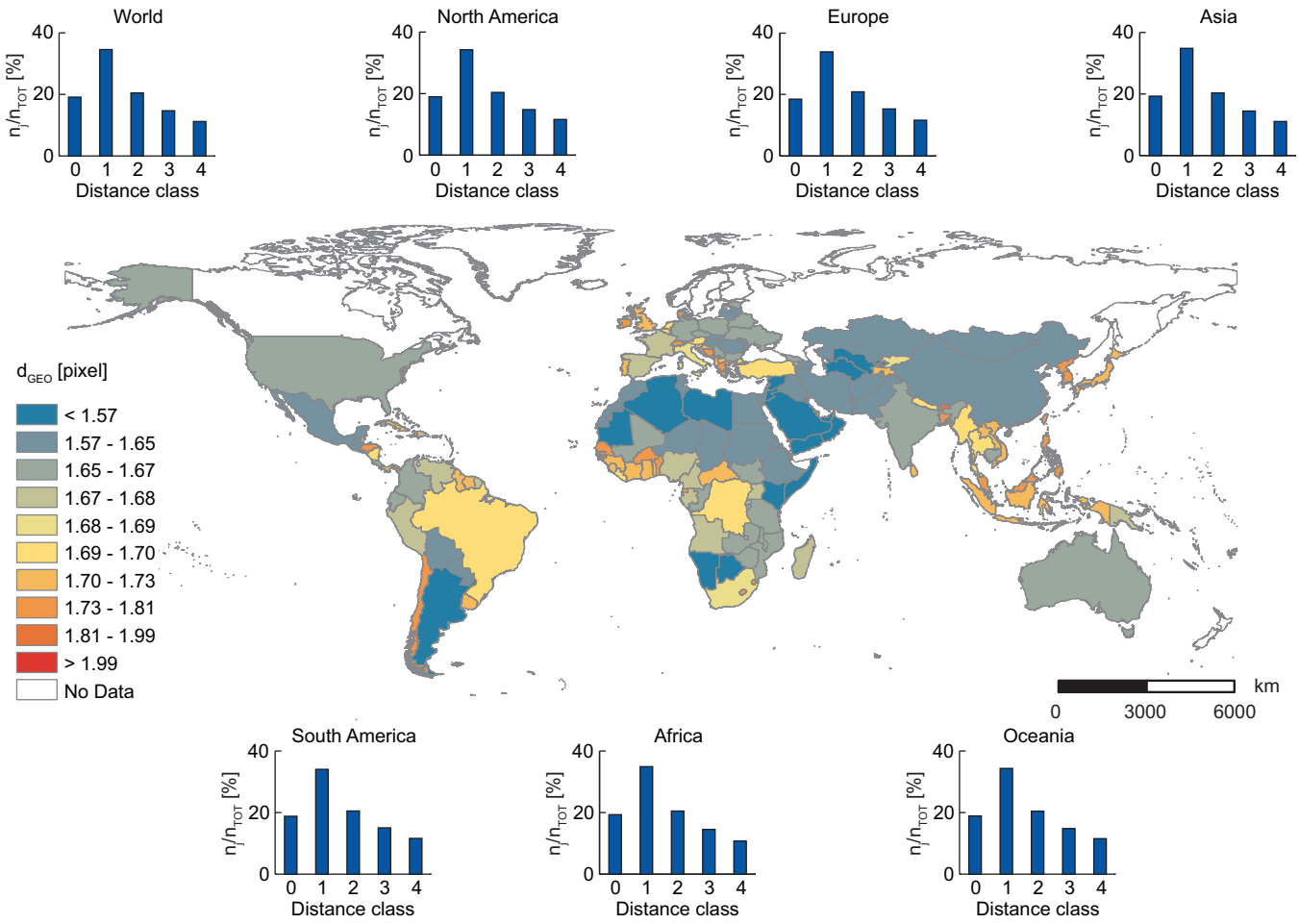

Figure 2. Country-based geographical proximity to the river network, $d_{GEO}(x)$, measured in pixel. Inset histograms show the geographical pixel distribution across the considered distance classes for the global and continental scales.

3 arc sec river network, and it can be considered representative of the main rivers at the global scale [*Lehner et al.*, 2006].

When analyzing the anthropogenic distribution for each study region and for each year, we found that $SOL_j(x,t)/SOL_{TOT}(x,t)$ histograms reproduce almost the same spatial trend as geographical ones (see inset histograms—yellow bars—for 2013 nightlights in Figure 3). Indeed, the majority of study regions are characterized by a hump-shaped trend with a mode for distance-1 class, whereas almost the same countries which made exception in the geographical distribution analysis (i.e., Bahamas, Bahrain, Guinea Bissau, Hong Kong, Malta, Sierra Leone, and Singapore) presented increasing nocturnal lights for increasing distance. The human distribution represented in terms of relative sum of nightlights clearly embeds intertwined information on (i) the anthropogenic presence and (ii) pixel distribution across distance classes, even though the geographical pattern seems to play a major role. We then excluded the distance class abundance $n_j(x)$ and focused only on average nightlight values $AOL_j(x,t)$. The $AOL_j(x,t) / \sum_{j=0}^{4} AOL_j(x,t)$ histograms reflect the inter-distance class variability of average nightlight values by assuming a characteristic nocturnal luminosity, $AOL_j(x,t)$, for each distance class. At the global and continental scales, the interclass distribution is characterized by a decreasing trend in average nightlights with increasing distance from the river network (see inset histograms—green bars—for 2013 nightlights in Figure 3). At the national scale, we distinguished four different interclass distribution trends, which did not present significant changes in the study period 1992–2013. More specifically, the majority of countries (nearly 71%) presented a decreasing pattern similar to the global and continental behavior, while increasing, constant and hump-shaped trends were found for the 19%, 6%, and 4% of study nations, respectively. Interestingly, the increasing trend is typical of countries from Central and South Africa, and South America (Figure 4).

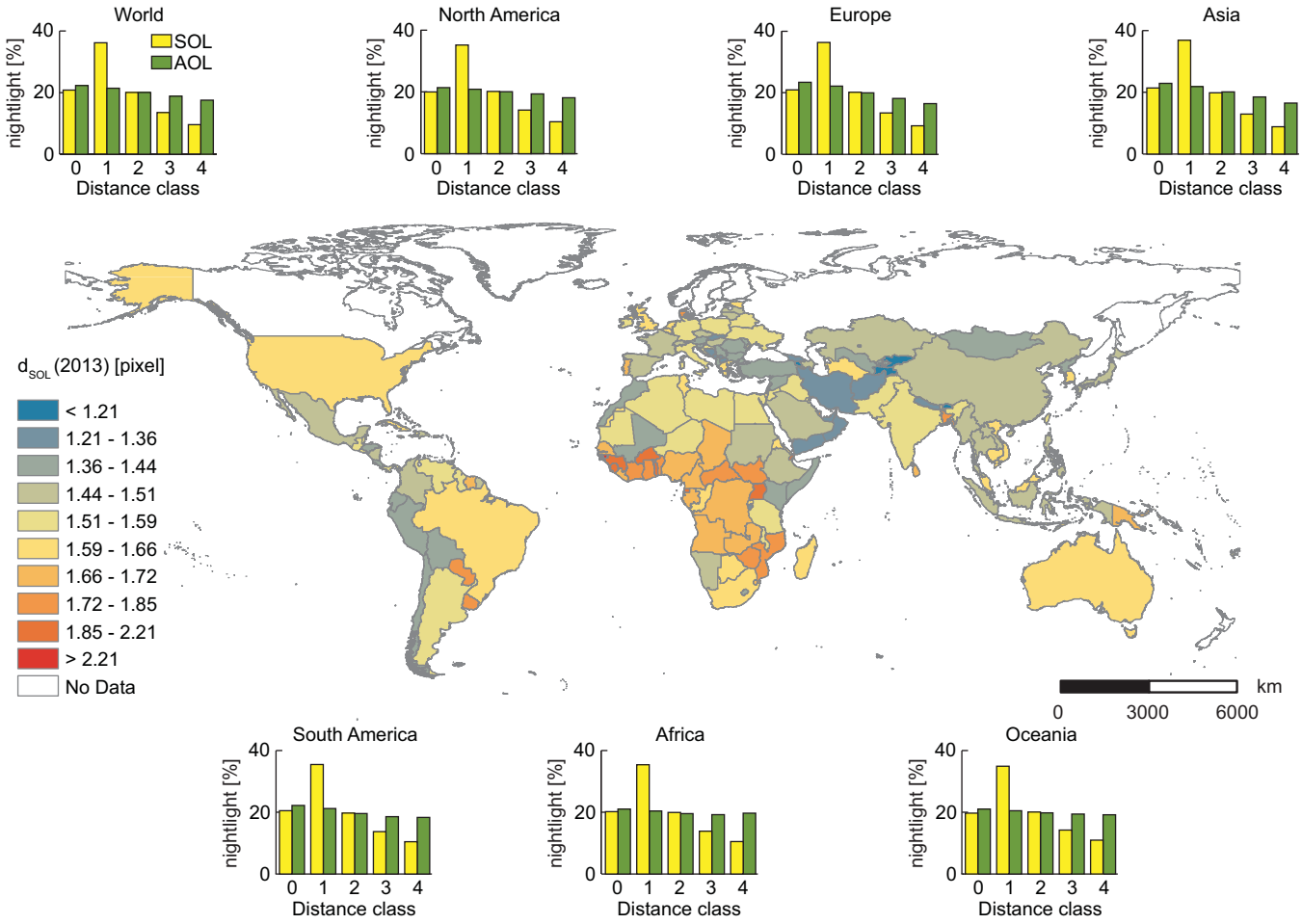

Figure 3. Country-based human proximity to the river network from 2013 nightlight values, $d_{SOL}(x, 2013)$, measured in pixel. Inset histograms show the nightlight distribution across the considered distance classes in terms of total (SOL, yellow bars) and average (AOL, green bars) nighttime lights for the global and continental scales.

As briefly mentioned before, the geographical distribution is exclusively based on the river network location across the globe, whereas the nightlight distribution provides information on population distribution across distance classes. When comparing these two distinct distributions (i.e., relative pixel luminosity versus relative pixel abundance) for each distance class and each year, interesting information revealing how human population is actually distributed can be found. Our results revealed that at the global scale the human-geographical ratio regularly decreases from distance-0 to distance-4 class (Figure 5). Indeed, the worldwide human-geographical ratio presents values greater than 1 for distance-0 and distance-1 classes, equal to 1.086 $\pm$ 0.005 and 1.044 $\pm$ 0.002, respectively (mean $\pm$ standard deviation evaluated for the whole study period), while the remaining classes are characterized by values smaller than 1 (0.979 $\pm$ 0.002, 0.900 $\pm$ 0.004, and 0.859 $\pm$ 0.005 for distance-2, distance-3, and distance-4, respectively). Our outcomes show that at the global scale the difference between, e.g., river pixels and distance-4 pixels are particularly significant, as outlined by a 30% decline in the human-geographical ratio. In fact, nearly a 6% decline of human density is associated to each distance class change when moving far from the river network, thus clearly pointing out a global preference of anthropogenic presence (i.e., settlements and economic activities) close to fluvial water bodies. In the study period from 1992 to 2013, the human-geographical ratio presents very minor temporal fluctuations within each distance class, which outline an overall unvarying temporal behavior of relative human distribution worldwide. Analogous spatiotemporal trends characterize the continental scale. More specifically, we identified the following two groups, based on similar human-geographical ratio values for each year and distance class. North America, Africa and Oceania belong to the first group, with ratios approximately equal to (mean $\pm$ standard deviation from 1992 to 2013) 1.050 $\pm$ 0.005, 1.020 $\pm$ 0.002, 0.980 $\pm$ 0.002, 0.950 $\pm$ 0.005, and 0.960 $\pm$ 0.005 for

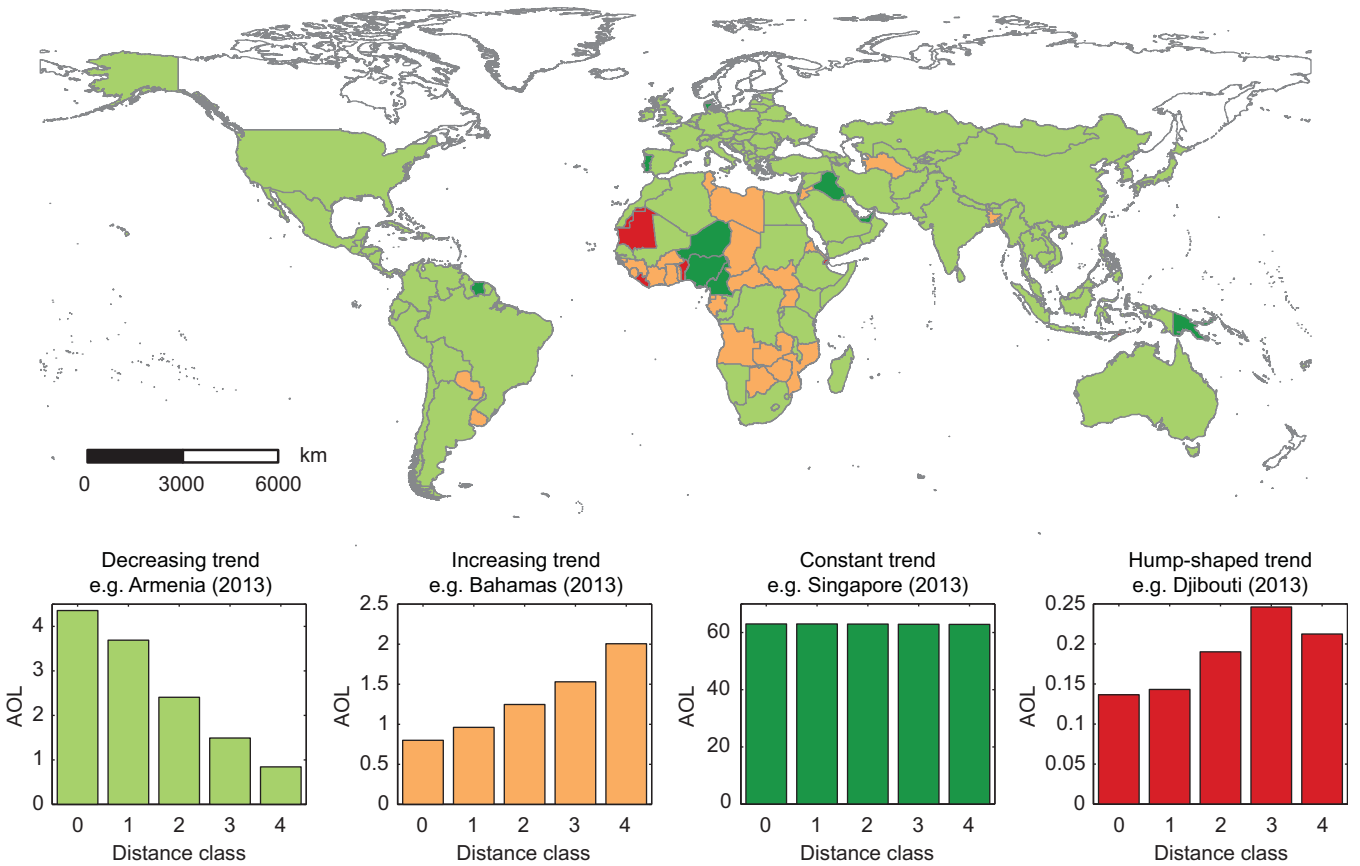

Figure 4. Country-based behavior of average 2013 nightlights, *AOL*(*x*,2013) distribution across distance classes: countries in light green, orange, dark green, and red present a decreasing, increasing, constant, and hump-shaped trend, respectively.

distance-0 to distance-4 classes, respectively, while Europe, Asia, and South America form the second group. The latter presents ratio values of nearly 1.110 ± 0.006, 1.050 ± 0.002, 0.980 ± 0.002, 0.890 ± 0.005, and 0.800 ± 0.005, for distance-0 to distance-4 classes, respectively, which reveal a more pronounced spatial variability among distance classes when compared to the first group (Figure 5). Indeed, within the study period the decline in the human-geographical ratio from river pixels to distance-4 pixels equals on average 8% and 38% for the first and the second group, respectively. At the national scale, the majority of the considered study regions shows a spatial trend similar to the global and continental ones, with again a human-geographical ratio greater than 1 for distance-0 and distance-1 classes, and values smaller than 1 for distance-2, distance-3 and distance-4 classes. This result clearly evidences that the majority of countries presents a higher human density close to streams and rivers with consequently relevant implications for the development of efficient ecosystem and flood management strategies. Nevertheless, we recognized a variability in human-geographical ratios among the considered study regions, e.g., with distance-0 and distance-1 values ranging from 1.05 to 2. Interestingly, from the temporal perspective some regions revealed fluctuations in ratio values, which can be reasonably associated to major historical events. A notable example is represented by Afghanistan (see Figure 5): from 1997 to 2000, i.e., during the Civil war, distance-0 and distance-1 ratio values showed a decline, while they slightly increased for distance-2 to distance-4 classes, thus disclosing that either major cities switched off nocturnal lights to avoid being bombed or that there has been a temporary shift of people from riverine and perifluvial areas to farther zones. Besides the aforementioned spatial trends, a few exceptions occurred. Several countries from Equatorial Africa (i.e., Nigeria, Benin, Togo, Ghana, Burkina Faso, Côte d'Ivoire, Guinea, Guinea Bissau, Equatorial Guinea, Gabon, Central African Republic, South Sudan, Eritrea, and Uganda) and from South East Africa (i.e., Botswana, Zambia, Zimbabwe, Mozambique), but also Paraguay, Uruguay, Jordan, Kuwait, Turkmenistan, and Bangladesh presented a spatial trend characterized by a higher human pressure far from rivers. For these regions, human-geographical ratios smaller than 1 are

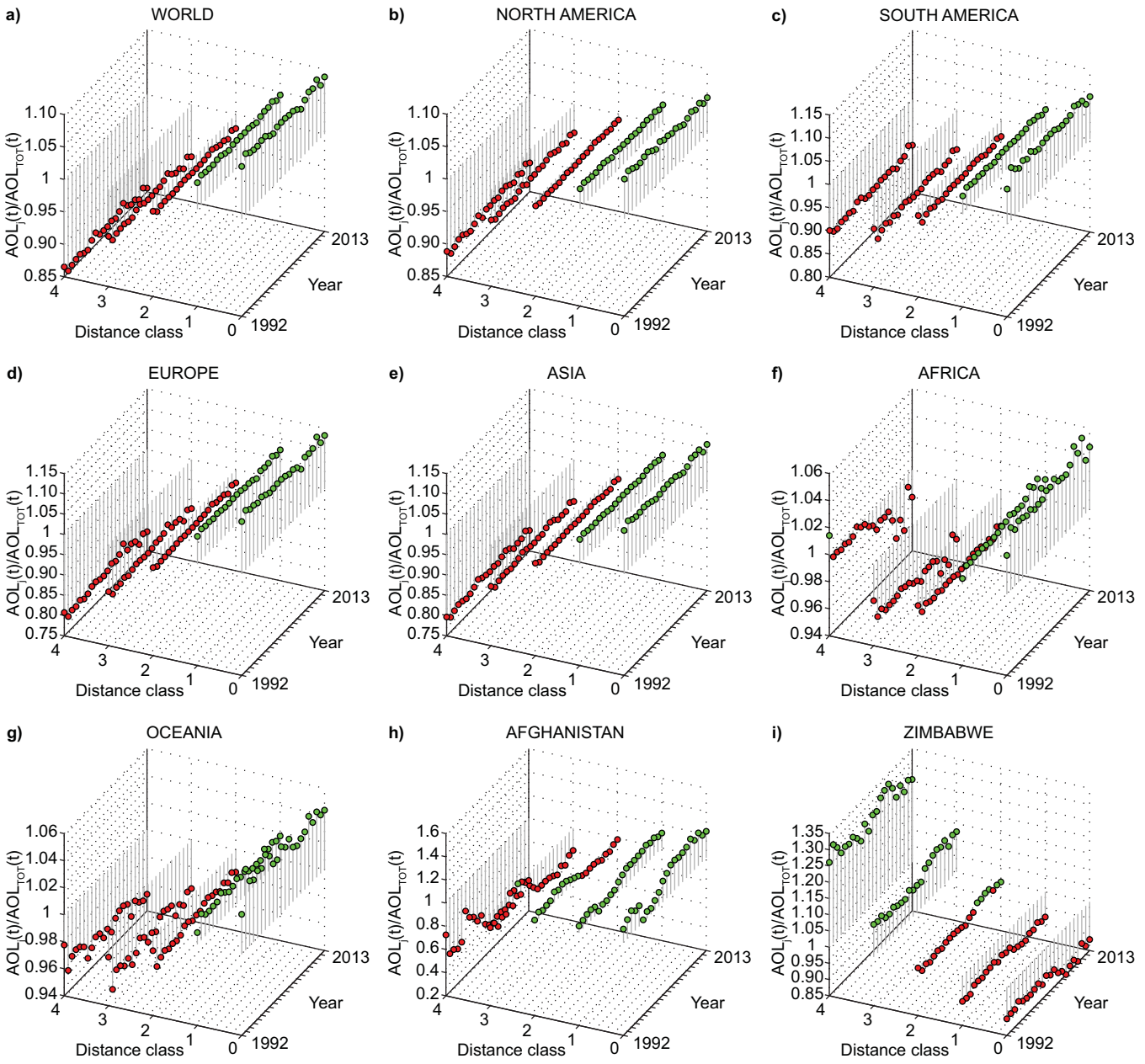

Figure 5. Human-geographical ratio for each study year from 1992 to 2013 and for each distance-from-rivers class. Positive values are represented with green dots, while negative values are marked in red. Gray bars show deviation from unitary values. (a–i) World, North America, South America, Europe, Asia, Africa, Oceania, Afghanistan, and Zimbabwe, respectively.

typical of distance-0 and distance-1 classes, whereas values greater than 1 belong to farther distance classes (see Figure 5).

4.2. Geographical and Human Proximity to the River Network

The average geographical proximity of randomly selected locations to the river network, $d_{GEO}(x)$, across the 175 study regions, which strictly depends on the delineation of the HydroSHEDS river network, spans between 1.38 and 2.49 pixels (Figure 2). At the global scale, the average geographical distance is equal to 1.64 pixels, while at the continental scale it is 1.62 pixels for Africa, 1.63 pixels for Asia, 1.66 pixels for North America, South America and Oceania, and 1.68 pixels for Europe.

From the human perspective, we assessed the average proximity of randomly selected individuals to rivers, $d_{SOL}(x,t)$, as derived from total nightlights (Figure 3). Within the study period, the average human proximity

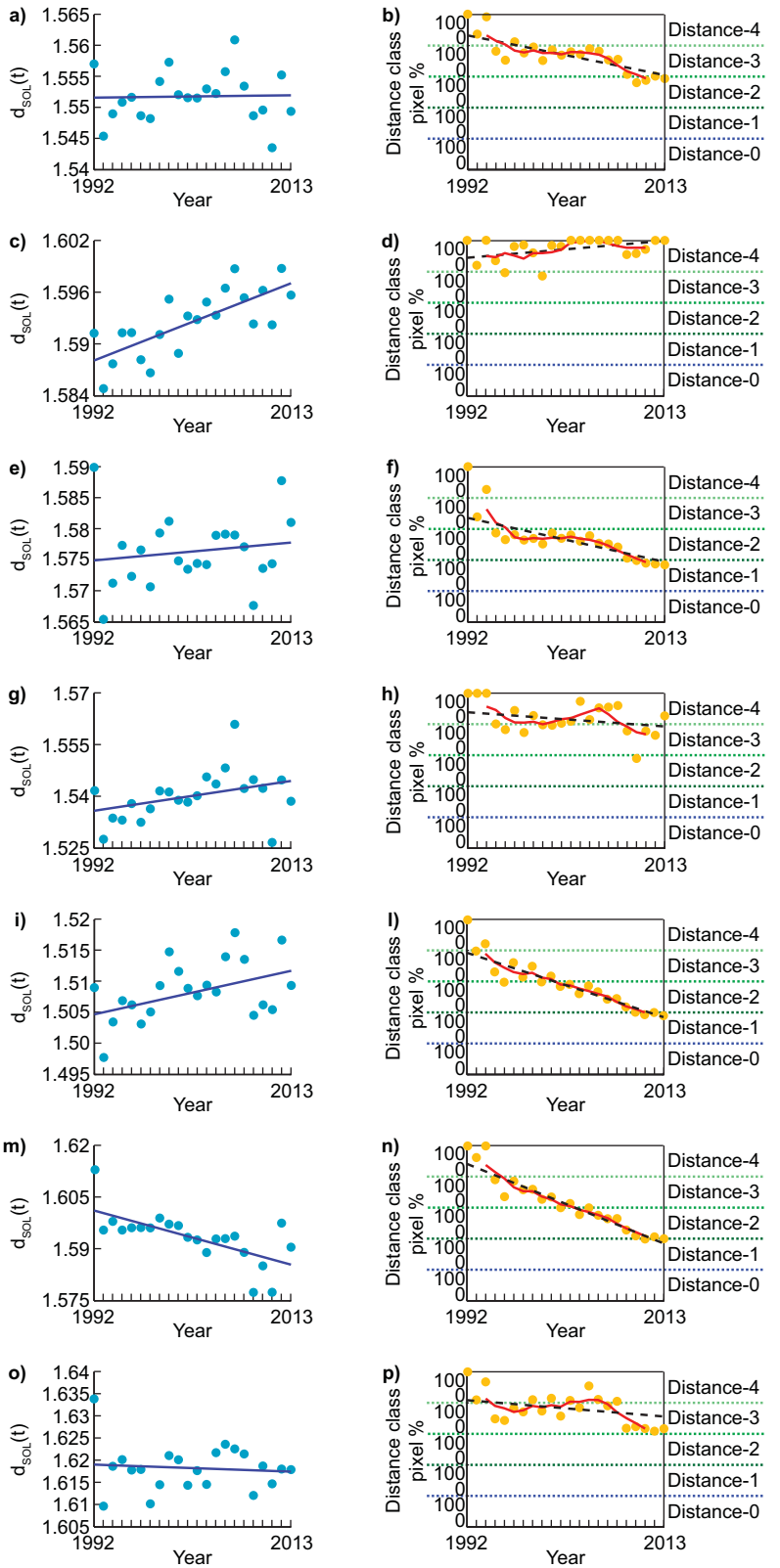

Figure 6. (left column) Temporal trends in average human proximity to rivers, $d_{SOL}(x,t)$ and (right column) human distance-from-river range, $D_{SOL^*}(x,t)$. Blue and orange dots represent computed values by using equations (7) and (10), respectively. Blue solid and black dashed lines identify the linear regression models described by equations (8) and (11), respectively. Red solid lines represent the 2 year centered moving average. (a and b) World, (c and d) North America, (e and f) South America, (g and h) Europe, (i and l) Asia, (m and n) Africa, and (o and p) Oceania. Regression line slope, intercept, correlation coefficient, and *p* values are reported in supporting information Table S1.

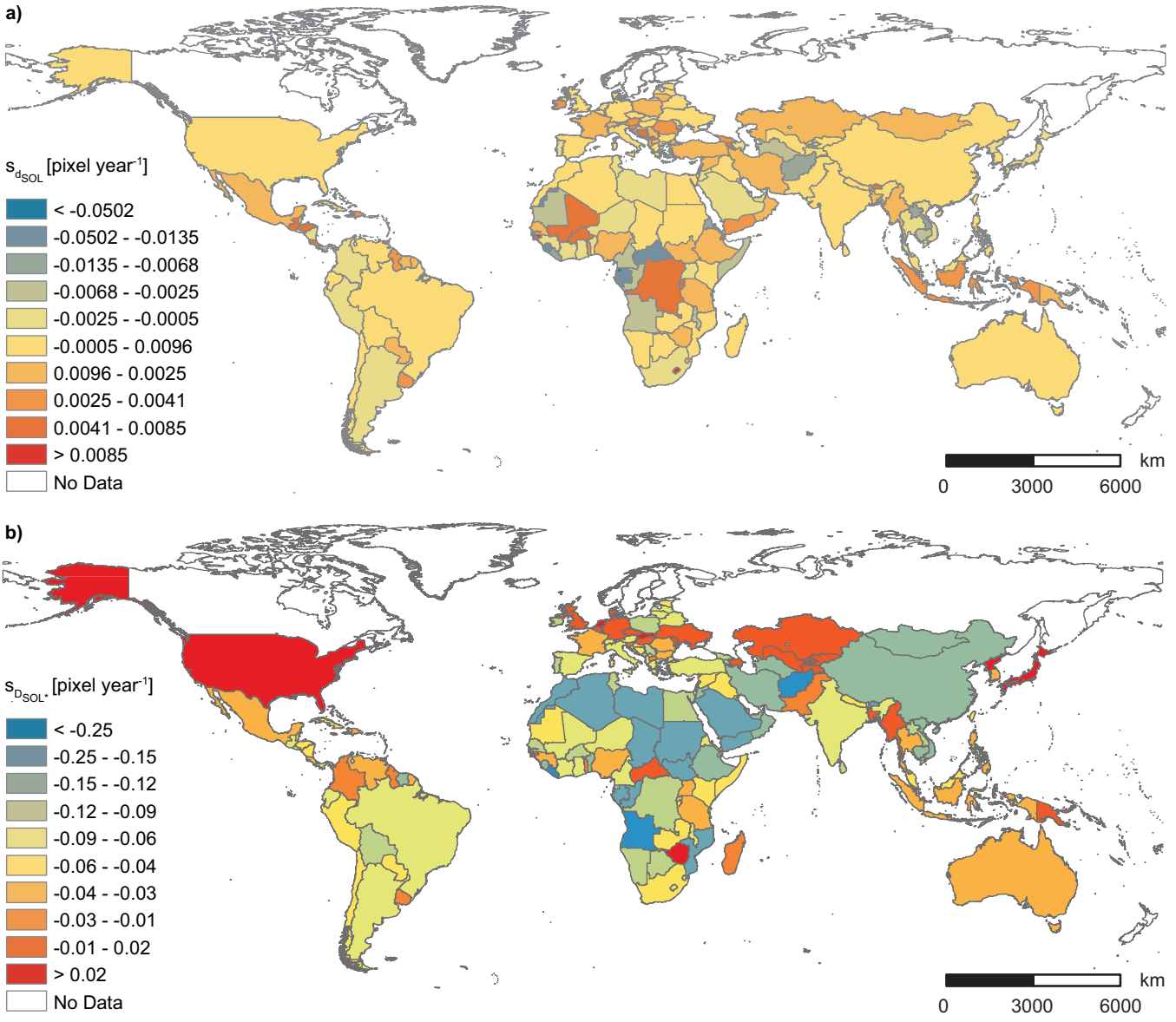

Figure 7. Country-based per year variation in (a) average human proximity to rivers $s_{d_{SOL}}(x)$ and (b) human distance-from-river range $s_{D_{SOL^*}}(x)$.

to rivers at the global scale equals 1.552 ± 0.004 pixels (mean and standard deviation computed from 1992 to 2013). At the continental scale, Asia, Europe, and South America show higher proximity values ($d_{SOL}(x)$ = 1.509 ± 0.005, 1.540 ± 0.007, 1.576 ± 0.006 pixels, respectively) compared to those characterizing North America, Africa, and Oceania ($d_{SOL}(x)$ = 1.593 ± 0.004, 1.593 ± 0.007, 1.618 ± 0.005 pixels, respectively). When we analyzed the average human proximity at the country scale, we observed relatively high values for Central America, the western part of South America, Asia, and Europe, whereas moderate to low proximities for North America, the eastern part of South America, South Africa, India, and Australia (Figure 3). Looking at the temporal evolution of the average human proximity to rivers, at the global and continental scales we found feeble temporal trends, almost negligible (i.e., $o10^{-4}$ pixel yr^{-1}), in the 22 year study period (Figure 6, left column and supporting information Table S1). At the country scale, even though a significant temporal tendency cannot be detected for nearly 60% of the study countries, visible trends characterized the remaining regions, which showed either a slightly enhanced (27 countries, see e.g., Gabon and Lao) or diminished (38 countries, see e.g., Honduras and Lesotho) proximity to streams and rivers (Figure 7a

and supporting information Table S1). Interestingly, Syria showed a severe decline in human proximity to rivers from 2012 to 2013 likely associated to the Syrian Crisis [*Li and Li*, 2014]. Overall, the analysis of the average human proximity of randomly selected individuals to rivers, $d_{SOL}(x,t)$, did not show significant temporal trends. This outcome clearly reflects the condition for which the percentage of total nightlights, $SOL_j(x,t)/SOL_{TOT}(x,t)$, across each distance class did not change in time. In other words, the human distribution expressed in terms of relative quantities remained overall constant from 1992 to 2013, thus seemingly contrasting with the idea that human population has moved closer to streams and rivers during recent years. However, we know that the human presence, expressed in terms of absolute quantities, presented a significant increment worldwide from 1992 to 2013, as observed by *Ceola et al*. [2014].

Therefore, in order to also incorporate information associated to absolute values of nightlights, and thus of human population and economic activity, we evaluated the human distance-from-river range, $D_{SOL^*}(x,t)$ by considering how the total sum of nightlights observed in 1992, i.e., $SOL_{TOT}(x,1992)=SOL^*(x)$, changed its spatial coverage across the study period (see equation (10)). Interestingly, we observed that the human distance-from-river range significantly decreased in the last 22 years, thus showing that the same human presence, which was originally located across all distance classes in 1992, has been found closer to fluvial water bodies in recent years. More specifically, when the entire globe is considered, the human distance-from-river range decreased at an average pace of 6.1×10^{-2} pixel yr^{-1}. Indeed, the human presence, represented by $SOL^*(x)$, from 1992 to 2013 moved from $D_{SOL^*}(1992)=4$ to $D_{SOL^*}(2013)=1.94$ pixels (Figure 6b and supporting information Table S1). Similarly, all continents showed declining human distance-from-river range values $D_{SOL^*}(x,t)$ from 1992 to 2013 (i.e., $o10^{-2}$ pixel yr^{-1}), with the only exception of North America, which presented an increasing temporal trend (Figure 6d and supporting information Table S1). From the national perspective, the majority of countries (i.e., nearly 84%) revealed a noticeable $D_{SOL^*}(x,t)$ decline within the study period (i.e., $o10^{-2}$ – $o10^{-1}$ pixel yr^{-1}), even though we encountered some exceptions showing a slightly increasing temporal trend (Figure 7b and supporting information Table S1). Decreasing trends in nightlights could be likely associated to increasing nocturnal luminosity, migration from rural to urban areas and expansion of cities along river corridors, while increasing trends could be explained by policies against nightlight pollution, like those already implemented in UK, USA, and Netherlands. Interestingly, for Moldova and Ukraine, the human population observed in 1992 within all distance classes was the maximum $SOL_{TOT}(x,t)$ value detected during the whole study period, thus resulting in a human distance-from-river range $D_{SOL^*}(x,t)$ constantly equal to 4. This outcome clearly reflects the economic crisis and the decline in total population from 1992 to 2013 in these two countries (i.e., −18% and −11% for Moldova and Ukraine, respectively) [*Worldbank*, 2015].

5. Discussion and Conclusions

In this paper, we investigated the temporal evolution of the anthropogenic presence and distribution across streams and rivers at the global scale. To this aim, we used worldwide images of nighttime lights (i.e., a proxy for human presence and economic activity) available on a yearly basis from 1992 to 2013 at a very detailed spatial resolution. We then associated nightlight values to the position of pixels located across five distinct distance classes.

Our approach, by performing global, continental, and country scale analyses, allowed not only for detailed observations of both geographical and anthropogenic spatial distribution, but, most importantly, it enabled us to detect temporal trends. Moving from the spatiotemporal distribution analysis, we then identified the average proximity to rivers, from both the geographical and the human perspective, by considering randomly selected locations and individuals, respectively. We also established the evolution in time of the human distance-from-river range, as described by the total sum of nightlights observed at the beginning of the study period (i.e., 1992).

Our results clearly pointed out an overall enhancement of human presence across the considered distance classes during the last 22 years, though presenting some differences among the considered study regions. In particular, we found significantly high human densities close to streams and rivers, whereas farther distance classes were characterized by smaller values, as shown by a 30% decline from river pixels to distance-4 pixels at the global scale.

When analyzing the average human proximity, our outcomes interestingly unraveled the absence of a significant temporal trend, which is clearly associated to an overall constant frequency distribution of total

nightlight values, and thus of human presence, within each distance class. However, when we analyzed how the 1992 human presence, settled across all the considered distance classes and represented by the total sum of nightlights, has changed its spatial distribution across the study period, we observed a significant temporal decline in the distance-from-river range, which clearly corresponds to a human presence enhancement. Indeed the same population which originally occupied the whole study area, from 1992 to 2013 started to settle increasingly closer to river bodies. Moreover, our analysis proved evidence of recent social conflicts and economic crisis, as exemplified by Syria, Afghanistan, Moldova, and Ukraine, which deserve to be considered when studying the dynamics of coupled human-water systems.

The present work, which places itself within the new generation of fine resolution remotely sensed data, along with the modern availability of extensive computing resources and data storage capacity, provides the exciting option to integrate at the global scale the local analyses of environmental features [*Richey et al*., 2015]. Such emerging perspective is particularly relevant for the analysis and mitigation of water stress and water-related threats. Indeed, the latter are often global problems that are originated by the sum of local impacts. For instance, local irrigation dominates the water use at the global scale. Solutions to these problems require large scale planning of local interventions and therefore a tight cooperation among institutions operating over a wide range of spatial scales. While in the past water resources management was mainly studied at the catchment scale, for the limited possibility to operate water transfers and large-scale planning, we are now given the opportunity to elaborate a vision for new solutions. The virtual water trade [*Hoekstra and Mekonnen*, 2012; *Carr et al*., 2012] gives an option to manage the water exchanges at a global scale by acting on the international trade of food products; at the same time, unprecedented connections between institutions allow one to coordinate the actions taken by local administrations, which are in charge of finding solutions to local problems.

To benefit from these exciting perspectives, the hydrological community needs to elaborate new concepts and new models, which should suitably incorporate the new high-resolution data made available by the recent advances in global monitoring techniques. There are opportunities for new model types that conceptualize processes in an integrated way, by taking advantage of coevolutionary principles of the geosystem, including the humans. Such models should be consistent with microscale physical laws and allow impact estimation at integrated scales [*Gleeson et al*., 2012; *Reager et al*., 2014; *Devineni et al*., 2015]. The increased complexity and breadth of such models demands for the use of information that goes beyond what is typically used in hydrology, with special emphasis on global remotely sensed data. It is therefore necessary for the hydrological community to devise new ideas for using unconventional observations in hydrological modeling.

We present in this paper an example: although nightlights provide an information that is not directly related to any hydrological process, we proved how these data can support both local and global analyses of water-related issues. Global information provides the opportunity for a radical evolution of water science through the integration of hydrological analyses over a wide range of scales.

Acknowledgments
The present work was developed within the framework of the Panta Rhei Research Initiative of the International Association of Hydrological Sciences. The data for this article are available at NOAA Earth Observation Group (http://ngdc.noaa.gov/eog/dmsp/downloadV4composites.html) and USGS HydroSHEDS (http://hydrosheds.cr.usgs.gov/index.php). Results derived from elaborations through a not-open-source code developed by the authors. More information can be gathered upon e-mail request to serena.ceola@unibo.it. S.C. and A.M. acknowledge the financial support from the EU funded project SWITCH-ON-603587. F.L. acknowledges support from the MIUR funded project RBFR12BA3Y. The authors thank Upmanu Lall and an anonymous reviewer for a constructive review of this paper.

References

Alfieri, L., P. Burek, E. Dutra, B. Krzeminski, D. Muraro, J. Thielen, and F. Pappenberger (2013), GloFAS—Global ensemble streamflow forecasting and flood early warning, *Hydrol. Earth Syst. Sci.*, *17*(3), 1161–1175, doi:10.5194/hess-17-1161-2013.

Barnett, T., et al. (2008), Human-induced changes in the hydrology of the western united states, *Science*, *319*(5866), 1080–1083, doi:10.1126/science.1152538.

Becker, A., and U. Grunewald (2003), Disaster management—Flood risk in central Europe, *Science*, *300*(5622), 1099, doi:10.1126/science.1083624.

Bennie, J., T. Davies, J. Duffy, R. Inger, and K. Gaston (2014), Contrasting trends in light pollution across Europe based on satellite observed night time lights, *Sci. Rep.*, *4*, 3789, doi:10.1038/srep03789.

Berghuijs, W., R. Woods, and M. Hrachowitz (2014), A precipitation shift from snow towards rain leads to a decrease in streamflow, *Nat. Clim. Change*, *4*(7), 583–586, doi:10.1038/nclimate2246.

Carr, J., P. D'Odorico, F. Laio, and L. Ridolfi (2012), On the temporal variability of the virtual water network, *Geophys. Res. Lett.*, *39*, L06404, doi:10.1029/2012GL051247.

Ceola, S., I. Hoedl, M. Adlboller, G. Singer, E. Bertuzzo, L. Mari, G. Botter, J. Waringer, T. Battin, and A. Rinaldo (2013), Hydrologic variability affects invertebrate grazing on phototrophic biofilms in stream microcosms, *PLoS ONE*, *8*(4), e60629, doi:10.1371/journal.pone.0060629.

Ceola, S., F. Laio, and A. Montanari (2014), Satellite nighttime lights revealing increased human exposure to floods worldwide, *Geophys. Res. Lett.*, *41*, 7184–7190, doi:10.1002/2014GL061859.

Chand, T., K. Badarinath, C. Elvidge, and B. Tuttle (2009), Spatial characterization of electrical power consumption patterns over India using temporal DMSP-OLS night-time satellite data, *Int. J. Remote Sens.*, *30*(3), 647–661, doi:10.1080/01431160802345685.

Chen, X., and W. Nordhaus (2011), Using luminosity data as a proxy for economic statistics, *Proc. Natl. Acad. Sci. U. S. A.*, *108*(21), 8589–8594, doi:10.1073/pnas.1017031108.

Crutzen, P. (2002), Geology of mankind, *Nature*, *415*(6867), 23, doi:10.1038/415023a.
Devineni, N., U. Lall, E. Etienne, D. Shi, and C. Xi (2015), America's water risk: Current demand and climate variability, *Geophys. Res. Lett.*, *42*, 2285–2293, doi:10.1002/2015GL063487.
Di Baldassarre, G., A. Viglione, G. Carr, L. Kuil, J. Salinas, and G. Bloeschl (2013), Socio-hydrology: Conceptualising human-flood interactions, *Hydrol. Earth Syst. Sci.*, *17*(8), 3295–3303, doi:10.5194/hess-17-3295-2013.
Di Baldassarre, G., A. Viglione, G. Carr, L. Kuil, K. Yan, L. Brandimarte, and G. Bloeschl (2015), Debates: Perspectives on sociohydrology: Capturing feedbacks between physical and social processes, *Water Resour. Res.*, *51*, 4770–4781, doi:10.1002/2014WR016416.
Elvidge, C., K. Baugh, E. Kihn, H. Kroehl, and E. Davis (1997), Mapping city lights with nighttime data from the DMSP operational linescan system, *Photogramm. Eng. Remote Sens.*, *63*(6), 727–734.
Elvidge, C., P. Sutton, T. Ghosh, B. Tuttle, K. Baugh, B. Bhaduri, and E. Bright (2009), A global poverty map derived from satellite data, *Comput. Geosci.*, *35*(8), 1652–1660, doi:10.1016/j.cageo.2009.01.009.
Erisman, J., G. Brasseur, P. Ciais, N. van Eekeren, and T. Theis (2015), Global change: Put people at the centre of global risk management, *Nature*, *519*, 151–153, doi:10.1038/519151a.
Gleeson, T., Y. Wada, M. Bierkens, and L. van Beek (2012), Water balance of global aquifers revealed by groundwater footprint, *Nature*, *488*(7410), 197–200, doi:10.1038/nature11295.
Gong, L., S. Halldin, and C. Xu (2011), Global-scale river routing-an efficient time-delay algorithm based on HydroSHEDS high-resolution hydrography, *Hydrol. Processes*, *25*(7), 1114–1128, doi:10.1002/hyp.7795.
Haddeland, I., et al. (2014), Global water resources affected by human interventions and climate change, *Proc. Natl. Acad. Sci. U. S. A.*, *111*(9), 3251–3256, doi:10.1073/pnas.1222475110.
Hirabayashi, Y., R. Mahendran, S. Koirala, L. Konoshima, D. Yamazaki, S. Watanabe, H. Kim, and S. Kanae (2013), Global flood risk under climate change, *Nat. Clim. Change*, *3*(9), 816–821, doi:10.1038/nclimate1911.
Hoekstra, A., and M. Mekonnen (2012), The water footprint of humanity, *Proc. Natl. Acad. Sci. U. S. A.*, *109*(9), 3232–3237, doi:10.1073/pnas.1109936109.
IPCC (2013), *Climate Change 2013: The Physical Science Basis. Contribution of Working Group I to the Fifth Assessment Report of the Intergovernmental Panel on Climate Change*, Cambridge Univ. Press, Cambridge, U. K.
Jaramillo, F., and G. Destouni (2014), Developing water change spectra and distinguishing change drivers worldwide, *Geophys. Res. Lett.*, *41*, 8377–8386, doi:10.1002/2014GL061848.
Jongman, B., P. Ward, and J. Aerts (2012), Global exposure to river and coastal flooding: Long term trends and changes, *Global Environ. Change*, *22*(4), 823–835, doi:10.1016/j.gloenvcha.2012.07.004.
Kummu, M., H. de Moel, P. Ward, and O. Varis (2011), How close do we live to water? A global analysis of population distance to freshwater bodies, *PLoS ONE*, *6*(6), e20578, doi:10.1371/journal.pone.0020578.
Kundzewicz, Z., et al. (2014), Flood risk and climate change: Global and regional perspectives, *Hydrol. Sci. J.*, *59*(1), 1–28, doi:10.1080/02626667.2013.857411.
Lehner, B., K. Verdin, and A. Jarvis (2006), HydroSHEDS technical documentation, technical report, World Wildlife Fund U.S., Washington, D. C. [Available at http://hydrosheds.cr.usgs.gov.]
Lehner, B., K. Verdin, and A. Jarvis (2008), New global hydrography derived from spaceborne elevation data, *Eos Tran. AGU*, *89*(10), 93–94, doi:10.1029/2008EO100001.
Li, X., and D. Li (2014), Can night-time light images play a role in evaluating the Syrian Crisis?, *Int. J. Remote Sens.*, *35*(18), 6648–6661, doi:10.1080/01431161.2014.971469.
Montanari, A., et al. (2013), "Panta Rhei-Everything Flows": Change in hydrology and society-The IAHS Scientific Decade 2013–2022, *Hydrol. Sci. J.*, *58*(6), 1256–1275, doi:10.1080/02626667.2013.809088.
Poff, N., J. Allan, M. Bain, J. Karr, K. Prestegaard, B. Richter, R. Sparks, and J. Stromberg (1997), The natural flow regime, *Bioscience*, *47*(11), 769–784, doi:10.2307/1313099.
Reager, J., B. Thomas, and J. Famiglietti (2014), River basin flood potential inferred using GRACE gravity observations at several months lead time, *Nat. Geosci.*, *7*(8), 589–593, doi:10.1038/NGEO2203.
Richey, A., B. Thomas, M. Lo, J. Famiglietti, S. Swenson, and M. Rodell (2015), Uncertainty in global groundwater storage estimates in a total groundwater stress framework, *Water Resour. Res.*, doi:10.1002/2015WR017351, in press.
Rockstrom, J., et al. (2014), The unfolding water drama in the Anthropocene: Towards a resilience-based perspective on water for global sustainability, *Ecohydrology*, *7*(5), 1249–1261, doi:10.1002/eco.1562.
Rogers, J. (Ed.) (2007), *Environmental and Water Resources: Milestones in Engineering History*, Am. Soc. of Civil Eng., Va.
Sivapalan, M., H. Savenije, and G. Bloeschl (2012), Socio-hydrology: A new science of people and water, *Hydrol. Processes*, *26*(8), 1270–1276, doi:10.1002/hyp.8426.
Slater, L., M. Singer, and J. Kirchner (2015), Hydrologic versus geomorphic drivers of trends in flood hazard, *Geophys. Res. Lett.*, *42*, 370–376, doi:10.1002/2014GL062482.
Small, C. (2004), Global population distribution and urban land use in geophysical parameter space, *Earth Interact.*, *8*, 1–18.
UNISDR (2013), *From Shared Risk to Shared Value The Business Case for Disaster Risk Reduction. Global Assessment Report on Disaster Risk Reduction*, U. N. Off. for Disaster Risk Reduct., Geneva, Switzerland.
Vorosmarty, C., P. Green, J. Salisbury, and R. Lammers (2000), Global water resources: Vulnerability from climate change and population growth, *Science*, *289*(5477), 284–288, doi:10.1126/science.289.5477.284.
Vorosmarty, C., et al. (2010), Global threats to human water security and river biodiversity, *Nature*, *467*(7315), 555–561, doi:10.1038/nature09440.
Voss, K., J. Famiglietti, M. Lo, C. de Linage, M. Rodell, and S. Swenson (2013), Groundwater depletion in the Middle East from grace with implications for transboundary water management in the Tigris-Euphrates-Western Iran region, *Water Resour. Res.*, *49*, 904–914, doi:10.1002/wrcr.20078.
Worldbank (2015), *World Bank Open Data*. [Available at http://data.worldbank.org/.]
Yamazaki, D., S. Kanae, H. Kim, and T. Oki (2011), A physically based description of floodplain inundation dynamics in a global river routing model, *Water Resour. Res.*, *47*, W04501, doi:10.1029/2010WR009726.

Erratum

1. Equation 5 had math information that was incorrect and has been corrected in this version.
2. A sentence on page 7071 was incorrect and has been corrected in this version. This version may be considered the authoritative version of record.